JPET Fast Forward. Published on January 29, 2021 as DOI: 10.1124/jpet.120.000417
This article has not been copyedited and formatted. The final version may differ from this version.

Glutathione S-Transferase P Influences Redox Homeostasis and Response to Drugs that Induce the Unfolded Protein Response in Zebrafish.

Leilei Zhang[1], Seok-Hyung Kim[2], Ki-Hoon Park[2], Zhi-wei Ye[1], Jie Zhang[1], Danyelle M. Townsend[3], Kenneth D. Tew[1]*

[1]Departments of Cell and Molecular Pharmacology and Experimental Therapeutics, Medical University of South Carolina, Charleston, South Carolina.

[2]Departments of Nephrology, Division of (Dept. of Medicine), Medical University of South Carolina, Charleston, South Carolina.

[3]Departments of Pharmaceutical and Biomedical Sciences, Medical University of South Carolina, Charleston, South Carolina.

JPET Fast Forward. Published on January 29, 2021 as DOI: 10.1124/jpet.120.000417
This article has not been copyedited and formatted. The final version may differ from this version.

Running Title:

Zebrafish Gstp1 drug response

[*]**Corresponding author:** Kenneth D. Tew, Department of Cell and Molecular Pharmacology and Experimental Therapeutics, Medical University of South Carolina, 70 President St., DD410, Charleston, SC 29425, USA.

E-mail: tewk@musc.edu Tel. 843-792-2514; Fax. 843-792-2475

Number of text pages: 25

Number of tables: 2

Number of figures: 7

Number of references: 42

Number of words in the Abstract: 158

Number of words in the Introduction: 564

Number of words in the Discussion: 837

List of abbreviations:

ANOVA, analysis of variance; atf, activating transcription factor 4; atf6, activating transcription factor 6; baxb, Bcl2 associated x b; bida, BH3-interacting domain death agonist a; bim, Bcl2 interacting mediator of cell death; bip: binding immunoglobulin protein; BMDDCs, bone marrow-derived dendritic cells; CDNB, 1-Chloro-2,4-dinitrobenzene; dnajc3, DnaJ homolog subfamily C member 3; ddit3 (chop), DNA damage-inducible transcript 3; DLAR, Division of laboratory animal resources; dpf, day post fertilization; edem1, ER degradation-enhancing alpha-mannosidase-like 1; ER, endoplasmic

JPET Fast Forward. Published on January 29, 2021 as DOI: 10.1124/jpet.120.000417
This article has not been copyedited and formatted. The final version may differ from this version.

reticulum; gadd45a, growth arrest and DNA-damage-inducible 45 alpha; gapdh, glyceraldehyde-3-phosphate dehydrogenase; gclc, glutamate-cysteine ligase catalytic subunit; gclm, glutamate-cysteine ligase modifier subunit; gr, glutathione reductase; grp94, glucose-regulated protein 94; GSH, glutathione; GSSG: GSH disulfide; GSTP, glutathione S-transferase Pi; hpf, hour post fertilization; IACUC, Institutional Animal Care and Use Committee; ire1, inositol-requiring protein-1; JNK, c-Jun N-terminal kinase; KO, knockout; LC_{50}, 50% lethal concentration; MAPK, mitogen-activated protein kinase; MEF, mouse embryo fibroblasts; MTC, maximum tolerable concentration; NO, nitric oxide; Nrf2, nuclear factor erythroid 2–related factor 2; PDI, protein disulfide isomerase; perk, protein kinase-like ER kinase; qPCR, quantitative polymerase chain reaction; ROS, reactive oxygen species; SD: standard deviations; SERCA, sarco/endoplasmic reticulum Ca^{2+}-ATPase; sod, superoxide dismutase; ThG, thapsigargin; TuM, tunicamycin; UPR, unfolded protein response; WISH, whole-mount *in situ* hybridization; WT, wild type; xbp1, X-box binding protein 1; xbp1-s, spliced form of xbp1; xbp1-u, un-spliced form of xbp1.

Section Recommendation: Cellular and Molecular

JPET Fast Forward. Published on January 29, 2021 as DOI: 10.1124/jpet.120.000417
This article has not been copyedited and formatted. The final version may differ from this version.

Abstract

We have created a novel *glutathione S-transferase Pi 1 (gstp1)* knockout (KO) zebrafish model and used it for comparative analyses of redox homeostasis, response to drugs that cause endoplasmic reticulum (ER) stress and induce the unfolded protein response (UPR). Under basal conditions, *gstp1* KO larvae had higher expression of antioxidant nuclear factor erythroid 2–related factor 2 (Nrf2) accompanied by a more reduced larval environment and a status consistent with reductive stress. Compared to wild type (WT), various UPR markers were decreased in KO larvae, but treatment with drugs that induce ER stress caused greater toxicities and increased expression of Nrf2 and UPR markers in KO; tunicamycin (TuM) and 0^2-{2,4-dinitro-5-[4-(N-methylamino) benzoyloxy] phenyl} 1-(N,N-dimethylamino) diazen-1-ium-1,2-diolate (PABA/NO) activated IRE1/XBP1 pathways, while thapsigargin (ThG) caused greater activation of PERK/ATF4/CHOP pathways. These results suggest that this teleost model is useful in predicting how GSTP regulates organismal management of oxidative/reductive stress and is a determinant of response to drug-induced ER stress and the UPR.

Significance Statement

A new zebrafish model has been created to study the importance of Gstp1 in development, redox homeostasis and response to drugs that enact cytotoxicity through ER-stress and induction of the UPR.

JPET Fast Forward. Published on January 29, 2021 as DOI: 10.1124/jpet.120.000417
This article has not been copyedited and formatted. The final version may differ from this version.

Introduction

Zebrafish have been used as surrogate species for predicting pharmacologically or toxicologically active compounds in man (Zon and Peterson, 2005). More than 50% of the enzymes involved in drug metabolism are conserved between zebrafish and humans (Li et al., 2010). Glutathione S-transferases (GST/*GST* (human protein/gene); Gst/*gst* (zebrafish protein/gene)) are a multifunctional family of enzymes with roles in phase II xenobiotic metabolism, ligand binding, kinase regulation and protein thiolase activities (Board and Menon, 2013), where substrate interactions involve a glutathione (GSH; G-site) and a substrate-binding site (H-site). Evolutionarily, GSTs are conserved throughout the plant and animal kingdoms, with three distinct sub-families, cytosolic, mitochondrial and microsomal (Frova, 2006), with cytosolic further divided into seven distinct classes, alpha, mu, omega, pi, theta, zeta, and sigma in mammals, or rho in teleost fish (Glisic et al., 2015). GST enzymatic activity is detected during the first 4 h of zebrafish development as well as in all adult organs. Two zebrafish *gstp* genes, *gstp1* and *gstp2* are syntenic with their human orthologues, but in zebrafish, *gstp1* is predominantly expressed during development, while *gstp2* is a minor constituent (Glisic et al., 2015). At the amino acid level, Gstp1 shares ~60% identity with Gstp1/GSTP1 from mouse/human and is perhaps the most versatile of the GST family, catalyzing GSH conjugation with select electrophilic chemicals, the forward reaction of protein S-glutathionylation (Townsend et al., 2009a; Zhang et al., 2018) and through protein–protein interactions, regulating c-Jun N-terminal kinase (JNK) mitogen-activated protein kinase (MAPK) signaling pathways (Okamura et al., 2015). GSTP has been found to be over-expressed in a range of human tumors (Howie et al., 1990) and mice lacking *gstp1/2* are more sensitive to chemicals that impact redox homeostasis (Henderson and Wolf, 2011) and also develop phenotypes of augmented immunity and increased myeloproliferation (Gate et al., 2004; Zhang et al., 2014). In addition to these intrinsic phenotypes, we have previously shown that GSTP contributes to redox regulation in the oxidative environment of the ER and that in turn, can

JPET Fast Forward. Published on January 29, 2021 as DOI: 10.1124/jpet.120.000417
This article has not been copyedited and formatted. The final version may differ from this version.

influence the UPR (Ye et al., 2017). This is relevant since certain drugs induce cytotoxicity through UPR induction with concomitant imbalance in redox homeostasis (Saito et al., 2009). The maintenance of redox homeostasis is crucial for the fate of vertebrates. Excess reactive oxygen species (ROS) or reducing equivalents can directly influence normal development and lead to pathologies (Grek and Townsend, 2014; Perez-Torres et al., 2017). As an inverse imbalance of oxidative stress, reductive stress (an excess of reducing equivalents), has emerged as an essential physiological parameter in both pro- and eukaryotes (Rajasekaran et al., 2007; Mavi et al., 2020). While the condition is characterized by elevated intracellular reducing equivalents, conversely by impacting mitochondrial functions and/or accumulating misfolding proteins in the ER (Peris et al., 2019; Wu et al., 2019), it can cause release of ROS, which can then activate Nrf2 (Guang et al., 2019).

In the present study, we used CRISPR gene editing to create *gstp1* KO zebrafish embryo/larvae, characterizing basal parameters of redox homeostasis and measured their comparative sensitivity to ER-stress and UPR-inducing drugs. Our data show that while *gstp1* KO fish develop normally they demonstrate increased sensitivities to drug-induced oxidative stress and ER stress. Moreover, endogenous baseline components of redox homeostasis were increased in *gstp1* KO larvae while the baseline expression of UPR proteins decreased. In this scenario, we reason that the absence of *gstp1* may enhance reductive stress, thereby influencing drug responses.

JPET Fast Forward. Published on January 29, 2021 as DOI: 10.1124/jpet.120.000417
This article has not been copyedited and formatted. The final version may differ from this version.

Materials and Methods

Zebrafish husbandry

Zebrafish (*Danio rerio*) were maintained at 28.5°C in a recirculating, filtered water system (Techiplast, USA) in reverse-osmosis-purified water supplemented with Instant Ocean salts (60 mg/L) on a 14-h light: 10-h dark lighting cycle and fed regular food twice per day (10 mg/fish/meal, the tested amount of food that can be completely consumed within 10 min). All methods for this article were performed in accordance with relevant guidelines and regulations of the NIH Guide for the Care and Use of Laboratory Animals and Medical University of South Carolina's Division of laboratory animal resources (DLAR) (Park and Kim, 2019). All experiments on zebrafish were approved by the Institutional Animal Care and Use Committee (IACUC) of the Medical University of South Carolina (IACUC protocol #3364).

Generation of *gstp1* KO zebrafish

Mix of guide RNA targeting exon3 in *gstp1* (GGACAAAGACCAGCAGCTGA, 50 ng/μL) and Cas9 RNA (100 ng/μL) was injected to 1-cell stage zebrafish embryos. Injected embryos were raised in the facility. F0 fish were outcrossed with wild type zebrafish and progeny with indels were identified by PCR (35 cycle, 64°C annealing temperature) with Forward (5'-CCTGGAATCATGTGCTCCCTGCAG-3') and Reverse (5'-ACAGGTGGCTTTCAAGTCGCCCT-3') primers and confirmed by sequencing. In this paper, we used mutant line with 11 bp deletions that resulted in premature stop at 33 amino acid loci.

Zebrafish toxicity tests

We used 4-day post fertilization (dpf) zebrafish larvae to determine acute toxicity because by this point, morphogenesis and the development of functioning primary organ systems is completed. In addition, *gstp1* expression remains constant throughout the larval stage. Drug concentrations

JPET Fast Forward. Published on January 29, 2021 as DOI: 10.1124/jpet.120.000417
This article has not been copyedited and formatted. The final version may differ from this version.

used in the acute toxicity tests are: Tunicamycin (TuM), 0, 2, 4, 6, 8, 10, 12 μM; Thapsigargin (ThG), 1, 0.5, 1, 1.5, 2, 2.5, 3 μM; 0^2-{2,4-dinitro-5-[4-(N-methylamino) benzoyloxy] phenyl} 1-(N,N-dimethylamino) diazen-1-ium-1,2-diolate (PABA/NO), 0, 2.5, 5, 7.5, 10, 12.5, 15 μM.. Larvae with >95% viability were chosen for experiments and randomly distributed into 24-well plates with 10 larvae per well and varying concentrations of drugs in triplicate wells for 24 hours. Zebrafish observations were made directly in the 24-well plate using an inverted dissecting microscope. Acute toxicity was further determined based on daily observations of abnormal abdomens, mild blood pooling/congestion and bent, short bodies. For the duration of the experiments, dead larvae were removed daily from the wells. Numbers of dead zebrafish within 24 hours for each drug concentration were recorded and survival rates (%) calculated. GraphPad Prism 5 (log [inhibitor] vs normalized response-variable slope nonlinear model) was used to calculate 50% lethal concentration (LC_{50}) values for each drug.

Quantitative polymerase chain reaction (qPCR)

For the qPCR studies, total RNA was isolated from 20 larvae/group with Trizol® Reagent (Invitrogen, Cat. 15596-026). The same amount of RNA was mixed to make pooled RNA as a template for complementary DNA synthesis. Oligo-dT primed complementary DNA was prepared by using superscript III First-Strand kit (Invitrogen, Cat.18080-051). Real-Time qPCR was performed with a Bio-rad, CFX96 Real-time system with 1 cycle of 98°C for 30 s, 45 cycles of 95°C for 15 s, and 60°C for 30 s using 50 ng cDNA, with 4 pmoles of each gene-specific primer per 20 μL reaction (Supplementary Table S1), and SsoAdvanced™ Universal SYBR® Green Supermix (Bio-rad, Cat. 172-5274). We used qPCR primers employed in a previous study (Park and Kim, 2019), or newly designed and tested. Glyceraldehyde-3-phosphate dehydrogenase (*gapdh*) was used as reference and relative quantification was calculated using double delta Ct method. The qPCR was assessed in at least triplicate replicates for each gene.

JPET Fast Forward. Published on January 29, 2021 as DOI: 10.1124/jpet.120.000417
This article has not been copyedited and formatted. The final version may differ from this version.

GST activity

GST activity was performed as previously described (Brautigam et al., 2018). 30 embryos (5 dpf), either control or treated with drugs, were collected and transferred to 300 µL of ice-cold homogenization buffer followed by gentle sonication on ice for 3×10 s with 10 s cooling in between (Fisher Scientific, CL-18). The lysates were centrifuged at 13,000 rpm for 10 min and supernatants collected and protein quantified using the BCA assay. The colorimetric GST activity assay was performed in a total volume of 100 µL at 22 °C in 0.1 M potassium phosphate buffer pH 7.5 with 5 mM GSH and 0.5 mM 1-Chloro-2,4-dinitrobenzene (CDNB), with absorbance once every 15 sec at 340 nm using a plate reader to obtain at least 18 time points. Enzymatic reactions were started by adding 50 µg homogenate and non-enzymatic background reaction rates were subtracted.

GSH and GSH disulfide (GSSG) levels

GSH and GSSG levels were measured as previously described (Park et al., 2019a). 30 embryos (5 dpf), either control or treated with drugs, were homogenized on ice in 300 µL of homogenization buffer. Protein determinations and protein concentrations were adjusted to 1 mg/mL, and then lysates were divided to two parts (for total thiol and GSH). One part was used to measure total thiol; the other part was subject to sulfosalicylic acid cell extraction (final 0.6%) to lyse the cells, placed at -80°C to freeze and thawed and centrifuged at 4000 g for 5 min to precipitate protein. The supernatants were kept for measuring reduced GSH; supernatants were neutralized (triethanolamine to the supernatant (1:16 ratio) to pH ~7. 2.5 µg of total thiol lysate or reduced GSH supernatant (volume to 10 µL) were added to thiol fluorescent probe IV (final 5 µM in PBS) and shaken for 15 min before reading fluorescent intensities at Ex/Em 400/465 nm. The concentration of thiol was quantified using GSH standards. Protein thiol can be measured by total thiol (reduced GSH + protein thiol) subtract by reduced GSH. For measuring GSSG, the

JPET Fast Forward. Published on January 29, 2021 as DOI: 10.1124/jpet.120.000417
This article has not been copyedited and formatted. The final version may differ from this version.

supernatant was incubated with the reduction system containing NADPH and glutathione reductase at 37 °C for 20 min. GSSG was calculated based on the results from reduced GSH and total thiol; the ratio of $GSH/GSSG = \frac{[GSH]}{([Total\ thiol]-[GSH])/2}$.

Intracellular ROS

Intracellular ROS was measured as previously described (Park et al., 2019b). 30 embryos (5 dpf) either control or drug treated were homogenized on ice in 300 µL of homogenization buffer. Protein concentrations were adjusted to 1 mg/mL and 25 µL transferred to 96-well plates suitable for fluorescence measurements. Fluorescence was measured at 480 nm excitation/530 nm emission. Details were essentially according to the manufacturer's instructions (Cell Biolabs, San Diego, CA). Each sample, including unknowns and standards, were assayed in triplicate.

Immunoblotting

Immunoblotting was performed as previously described (Zhang et al., 2019). 30 embryos (5 dpf) either control or treated with drugs, were collected and transferred to 300 µL of ice-cold homogenization buffer followed by gentle sonication on ice for 3×10 s with 10 s cooling in between. The lysate was centrifuged at 16000 g for 10 min, supernatant collected, and protein quantified using the BCA assay. Equal amounts (60 µg) of protein were electrophoretically separated by SDS PAGE (Bio-Rad) and transferred onto low fluorescent polyvinylidene fluoride membranes (Millipore) by the Trans-Blot Turbo Transfer System (Bio-Rad). PVDF was incubated in the Odyssey blocking buffer (LI-COR) for 1 hour to reduce non-specific binding and then probed with appropriate primary antibodies at 4°C overnight. Immunoblots were then developed with infrared (IR) fluorescence IRDye secondary antibodies (LI-COR) at a dilution of 1:15,000, imaged with a 2-channel (red and green) IR fluorescent Odyssey CLx imaging system (LI-COR) and quantified with ImageJ software (FIJI).

JPET Fast Forward. Published on January 29, 2021 as DOI: 10.1124/jpet.120.000417
This article has not been copyedited and formatted. The final version may differ from this version.

Statistical analysis

All measurements were collected from at least 3 independent experiments. Statistical analysis was performed using GraphPad Prism 6.0 and Microsoft Excel. Significant differences were determined using 2 tailed t tests and one-way analysis of variance (ANOVA) followed by Newman-Keuls as a post-test.

JPET Fast Forward. Published on January 29, 2021 as DOI: 10.1124/jpet.120.000417
This article has not been copyedited and formatted. The final version may differ from this version.

Results

Zebrafish contain two homologs of human GSTP1

The annotated zebrafish genome (GRCz11, www.ensembl.org) confirmed that *gstp* exists as two genes, *gstp1* and *gstp2* that share high amino acid identities (87%), each located on chromosome 14. These two isoforms (NM_131734.3, *gstp1*; and NM_001020513.1, *gstp2*) share ~60% identity at the amino acid level with the human homologue GSTP1, found on chromosome 11 (Supplemental Fig. S1). During embryo development, *gstp1* is expressed in all organs, while *gstp2* is below the levels of standard detection. Gstp1 is also the most prevalent and abundant of the zebrafish GST isozymes.

Generation and characterization of *gstp1* mutant zebrafish.

CRISPR/Cas9 targeting *gstp1* caused an 11 bp deletion in exon 3 of *gstp1*, which led to a stop codon at the 33 amino acid locus (Fig. 1A). Loss of functional *gstp1* did not alter the gross morphology of either embryos or larvae (Supplemental Fig. S2A). There were no obvious defects during embryogenesis, hatching or early adult growth, with normal survival and fecundity, circumstances similar to *gstp1/2* KO mice (Henderson et al., 1998). Since *gstp1/2* KO mice have hematopoietic changes, we performed *in situ* hybridization against globin, a marker for erythrocytes, revealing no significant changes in the number of red blood cells in *gstp1* KO embryos (Supplemental Fig. S2B). Expression of *gstp1* remains constant from hatching until the late larval stages, so to measure any functional consequences of the KO, 4 dpf larvae of each genotype were assessed for expression of the *gstp* gene and protein and enzyme activity. Gene and protein expression were absent in the KO larvae, which also showed lower GST activity levels (Fig. 1B-D), where residual CDNB activity will be a consequence of the other GST isozymes.

Drug sensitivities in WT and *gstp1* KO larvae.

JPET Fast Forward. Published on January 29, 2021 as DOI: 10.1124/jpet.120.000417
This article has not been copyedited and formatted. The final version may differ from this version.

Larvae were exposed to three drugs known to cause ER stress, albeit by distinct mechanisms, TuM, ThG and PABA/NO. Lethality curves are presented in Figure 2. 4 dpf from WT and *gstp1* KO larvae were used to ascertain maximum tolerable concentration (MTC) of the drugs. These values were 10 μM (TuM), 2.5 μM (ThG) and 12.5 μM (PABA/NO). For subsequent experiments, concentrations decreasing geometrically from the MTC were used and the LC_{50} values shown in Table 1. Despite the differences in drug administration conditions, these values are comparable with those for *gstp1/2* KO cells and mice, and *phosphomannomutase 2* (*PMM2*) mutation zebrafish larvae (Table 1) (Ye et al., 2017; Mukaigasa et al., 2018; Cheng et al., 2019; Liu et al., 2019; Xia et al., 2020). Overall, the data showed that deletion of *gstp1* enhances the cytotoxic effects of TuM, ThG or PABA/NO.

Malformation caused by drugs in WT and *gstp1* KO larvae.

Using bright-field microscopy, we identified no apparent differences in development between WT and KO early larvae (Fig. 3A). Following 16-h drug treatments, the majority of the KO larvae showed significant pericardial edema and curvature of spine and tail (ThG); pericardial edema and yolk sac edema (PABA/NO). However, in WT larvae these effects were absent or mild in nature (Fig. 3A&B). Following 24-h treatments, excess malformation caused by ThG and PABA/NO occurred in a time dependent manner, the effects in WT larvae remained less substantial than in KO (Fig. 3D&E). Distinct from the other two drugs, TuM caused no malformations before 24 h, at which time, pericardial edema was more pronounced in KO than WT larvae (Fig. 3A&B; D&E). However, overall body lengths were unaffected by any of the drugs (Fig. 3C&F). Thus, at most of the treatment time points, TuM had a diminished impact on ratios of abnormal vs normal development features compared to either ThG or PABA/NO.

Impact of *gstp1* KO phenotype on redox pathways.

JPET Fast Forward. Published on January 29, 2021 as DOI: 10.1124/jpet.120.000417
This article has not been copyedited and formatted. The final version may differ from this version.

We reasoned that basic parameters of GSH homeostasis were likely to be altered by GSTP deletion. As such, we compared WT and *gstp1* KO larvae for alterations in expression of redox pathway constituents, both before and after drug treatments. Figures 4-6 illustrate that *gstp1* KO larvae had: increased baseline values for GSH, protein thiol, GSH/GSSG ratios and gene expression of *glutamate-cysteine ligase catalytic subunit* (*gclc)* and *glutathione reductase* (*gr)* and decreased GSSG and ROS levels (Fig. 4); increased gene expression of *nrf2a*, *sod2* (Fig. 5 and Table 2); higher baseline expression of Nrf2 protein and increased Nrf2 and SOD1 protein levels following each drug (Fig. 6). Drug treatments produced a coordinated increase in GSH (Fig. 4A, G, M); protein thiol (Fig. 4D, J, P); ratios of GSH/GSSG (Fig. 4C, I, O); ROS (Fig. 4E, K, Q); and gene expression of *gclc, glutamate-cysteine ligase modifier subunit (gclm)* and *gr* (Fig. 4F, L, R); and decreased GSSG (Fig. 4B, H, N). The shift in the ratio of GSH/GSSG toward a more reduced state, plus the presence of higher ROS in *gstp1* KO larvae following drug treatments would be consistent with some form of reductive stress preceding resultant increases in oxidative stress.

ER stress/UPR gene and protein expression patterns.

In both mice and zebrafish, *gstp1* gene expression is influenced by induced ER stress (Ye et al., 2017) (Mukaigasa et al., 2018), so we compared drug effects in the WT and KO larvae. We chose UPR sensors and their target genes, as well as subsequent genes associated with mitochondrial injury and ER stress-induced apoptosis (*baxb*, *bida* and *bim*). Relative to WT larvae, *gstp1* KO was linked with lower baseline expressions of: *bip* (0.51-fold), *ire1* (0.73-fold), *atf6* (0.35-fold), *xbp1-u* (0.80-fold), *xbp1-s* (0.61-fold), *atf4* (0.79-fold), *chop* (0.70-fold) and *gadd45a* (0.74-fold), indicating connectivity between *gstp1* and UPR in zebrafish (Fig. 5, Table 2). In both WT and KO larvae, TuM and PABA/NO produced a coordinated increase in expression of UPR-associated genes including, *bip*, *dnajc3*, *grp94*, *ire1*, *xbp1-u*, *xbp1-s*, *atf4*, *chop*, *gadd45a*, *edem1*, *baxb*, *bida* and *bim*. In addition, significant induction of *gadd45a* was found in KO larvae, while TuM and PABA/NO decreased its expression in WT larvae. However, in the KO larvae, ThG enhanced

JPET Fast Forward. Published on January 29, 2021 as DOI: 10.1124/jpet.120.000417
This article has not been copyedited and formatted. The final version may differ from this version.

expression of *bip*, *dnajc3*, *grp94*, *perk*, *atf4*, and *chop*; diminished the upregulation of *ire1*, *edem1*, *baxb*, *bida* and *bim.* These data confirmed that manipulation of *gstp1* expression directly influenced ER stress/UPR in zebrafish.

Immunoblots identified key UPR protein expression differences between WT and *gstp1* KO larvae (Supplemental Fig. S3). *Gstp1* KO was associated with lower baseline expression of IRE1 and XBP1s. Figure 7 shows that drug treatments produced a coordinated increase in all UPR proteins, except IRE1 and XBP1-s. Independent of baseline expression patterns, TuM and PABA/NO significantly increased IRE1, XBP1-s and Bax in *gstp1* KO larvae, while ThG decreased their expression, but increased CHOP. Induction of BiP was caused by each of the three drugs in both WT and KO larvae. These results indicate while minor differences for each drug exist, in general, the absence of *gstp1* makes the larvae more vulnerable to ER stress/UPR. Consistent with the toxicity assays and gene expression data, drug treatments induced oxidative and ER stress for the majority of the markers of interest in KO larvae, particularly the IRE1/XBP1 UPR pathway for TuM and PABA/NO, and the PERK/ATF4/CHOP pathway for ThG.

JPET Fast Forward. Published on January 29, 2021 as DOI: 10.1124/jpet.120.000417
This article has not been copyedited and formatted. The final version may differ from this version.

Discussion

Since zebrafish are useful surrogates for the study of certain aspects of human drug response (Ding et al., 2020; Mohd Sakeh et al., 2020), our goal with the present work was to generate and characterize a novel *gstp1* deficient model to establish its role in redox homeostasis and drug response. Zebrafish Gstp1 shares with human GSTP1 conserved residues in the substrate binding site (H-site), including Tyr^{8}, Phe^{9}, Val^{11}, Ile^{105} and Tyr^{109} (Suzuki et al., 2005) each important in GSH-conjugation with various substrates (Maher, 2005). During the developmental process, the physiological roles of Gstp1 are well conserved among vertebrates, including teleost fish and mammals (Abunnaja et al., 2017). Unlike mammals that express both GSTP1 and GSTP2 in a tissue specific manner, in zebrafish, Gstp1 is the predominant isoenzyme of this class and it is constitutively expressed at high levels in all tissues, especially throughout early development, while Gstp2 is essentially undetectable (Glisic et al., 2015). Gstp2 does have a high catalytic constant for CDNB (Glisic et al., 2015) and this accounts for the residual CDNB activity we measured in *gstp1* KO larvae. Gstp1 was expressed early during zebrafish embryogenesis, similar to GSTP1 in mammalian embryogenesis (Raijmakers et al., 2001; Tierbach et al., 2018), implying that Gstp1 shares similar functions in both. Homozygous zebrafish mutants were fertile and displayed no overt morphological phenotypes under normal rearing conditions. As with mice, *gstp1/2* KO was not embryonic lethal, nor was there any intrinsic impact on early embryonic development or growth patterns. However, our results revealed that *gstp1* KO larvae did contain higher basal levels of GSH, GSH/GSSG and Nrf2, with lower levels of basal ER stress, evidenced by decreases in expression of UPR-associated proteins, suggestive of conditions of reductive stress in these larvae.

Abrogation of *gstp1/2* in mice was shown to cause increased ER stress and enhanced sensitivity to various drugs through activation of the UPR (Ye et al., 2017) and compared to the KO cells, WT *gstp1/2* bone marrow dendritic cells (BMDDC) were more resistant to these drugs (Zhang et

JPET Fast Forward. Published on January 29, 2021 as DOI: 10.1124/jpet.120.000417
This article has not been copyedited and formatted. The final version may differ from this version.

al., 2020). Consistent with the mouse data, *gstp1* KO zebrafish larvae were shown to be more sensitive than WT larvae to TuM, ThG and PABA/NO. TuM is an N-linked glycosylation inhibitor, causing accumulation of misfolded proteins in the ER resulting in UPR (Oda et al., 2008) and also actuates GSTP translocation from the cytosol to the ER (Ye et al., 2017). TuM shifted the ratio of GSH/GSSG towards the more reduced state, producing reductive stress-induced mitochondrial dysfunction and ROS augmentation, thereby increasing Nrf2, IRE1, XBP1-s and Bax expression. Taken together, these results suggest that *gstp1* protects larvae from oxidative and ER stress and death via IRE1/XBP1/Bax pathway, implicating *gstp1* in pathways relevant to reductive stress, where its absence enhances reductive stress induced cell death.

ThG is an inhibitor of the Ca^{2+} ATPase (SERCA), causing disruption of Ca^{2+} homeostasis and UPR (Sehgal et al., 2017). Cells from *gstp1/2* KO mice showed increased sensitivity to ThG (Ye et al., 2017). Our present results showed that although ThG was more cytotoxic and induced oxidative and ER stress in *gstp1* KO larvae, its effects were distinct from TuM. Instead of activating IRE1/XBP1 axis, ThG increased expression of PERK, ATF4 and CHOP compared to WT larvae, confirming a distinct mechanism of action. PABA/NO is a GST-activated prodrug that releases nitric oxide (NO) causing nitrosative and oxidative stress that in mice targets protein disulfide isomerase (PDI) causing accumulation of misfolded proteins and activation of the UPR (Townsend et al., 2009b; Xiong et al., 2012). Our results showed PABA/NO, to some extent, mimicked TuM in *gstp1* KO larvae. For example, in *gstp1* KO larvae it was more cytotoxic, increased GSH levels and GSH/GSSG ratios and ROS and raised levels of Nrf2, IRE1, XBP1-s and Bax. Activation of PABA/NO may have been influenced by the absence of *gstp1*, but over the long incubation period, spontaneous and other GST isoform activation will have compensated (Townsend et al., 2009b). With respect to drug induced developmental effects, at 24-h time point, exposure of larvae to either TuM or PABA/NO caused pericardial edema, while ThG caused severe pericardial edema and curvature of the spine and tail (Figure 3D), again reflecting the

distinctive mechanisms of action. Although deficiencies in *gstp1/2* in mice have been linked with altered hematopoiesis (Gate et al., 2004) in zebrafish the unaltered hemoglobin results suggest dissimilarities between the species. This may be explained by the indications that microsomal GST (Brautigam et al., 2018) and a melanin umbrella, rather than bone has a more specific role in regulation of teleost marrow functions (Kapp et al., 2018).

Overall, our results indicate that *gstp1* KO larvae are more susceptible to UPR following TuM, ThG or PABA/NO, although the basal levels of UPR in *gstp1* KO larvae are significantly lower than those in WT larvae. Taken together, this new zebrafish model has enabled us to clarify the roles of *gstp1* in redox homeostasis and drug and stress response and show that while there are some differences from mammals, there are also significant similarities.

Acknowledgments

This work was supported by grants from the National Institutes of Health (CA08660, CA117259, NCRR P20RR024485 - COBRE in Oxidants, Redox Balance and Stress Signaling) and support from the South Carolina Centers of Excellence program and was conducted in a facility constructed with the support from the National Institutes of Health, Grant Number C06 RR015455 from the Extramural Research Facilities Program of the National Center for Research Resources. Supported in part by the Drug Metabolism and Clinical Pharmacology shared resource, Hollings Cancer Center, Medical University of South Carolina.

Author Disclosure Statement

No author has an actual or perceived conflict of interest with the contents of this article.

Authorship Contributions

Participated in research design: Tew, Townsend.

Conducted experiments: Ye, Zhang (L), Kim.

Contributed new reagents or analytic tools: Kim, Park, Zhang (J).

Performed data analysis: Zhang (L).

Wrote or contributed to the writing of the manuscript: Tew, Zhang (L), Kim.

References

Abunnaja MS, Kurogi K, Mohammed YI, Sakakibara Y, Suiko M, Hassoun EA and Liu MC (2017) Identification and characterization of the zebrafish glutathione S-transferase Pi-1. *J Biochem Mol Toxicol* **31**.

Ali BH, Al-Salam S, Adham SA, Al Balushi K, Al Za'abi M, Beegam S, Yuvaraju P, Manoj P and Nemmar A (2019) Testicular Toxicity of Water Pipe Smoke Exposure in Mice and the Effect of Treatment with Nootkatone Thereon. *Oxid Med Cell Longev* **2019**:2416935.

Board PG and Menon D (2013) Glutathione transferases, regulators of cellular metabolism and physiology. *Biochim Biophys Acta* **1830**:3267-3288.

Brautigam L, Zhang J, Dreij K, Spahiu L, Holmgren A, Abe H, Tew KD, Townsend DM, Kelner MJ, Morgenstern R and Johansson K (2018) MGST1, a GSH transferase/peroxidase essential for development and hematopoietic stem cell differentiation. *Redox Biol* **17**:171-179.

Cheng FY, Lee YH, Hsu YH, Chiu IJ, Chiu YJ, Lin YF and Chiu HW (2019) Promising therapeutic effect of thapsigargin nanoparticles on chronic kidney disease through the activation of Nrf2 and FoxO1. *Aging (Albany NY)* **11**:9875-9892.

Ding Y, Yang J, Chen P, Lu T, Jiao K, Tester DJ, Giudicessi JR, Jiang K, Ackerman MJ, Li Y, Wang DW, Lee HC, Wang DW and Xu X (2020) Knockout of SORBS2 Protein Disrupts the Structural Integrity of Intercalated Disc and Manifests Features of Arrhythmogenic Cardiomyopathy. *J Am Heart Assoc* **9**:e017055.

Frova C (2006) Glutathione transferases in the genomics era: new insights and perspectives. *Biomol Eng* **23**:149-169.

Gate L, Majumdar RS, Lunk A and Tew KD (2004) Increased myeloproliferation in glutathione S-transferase pi-deficient mice is associated with a deregulation of JNK and Janus kinase/STAT pathways. *J Biol Chem* **279**:8608-8616.

Glisic B, Mihaljevic I, Popovic M, Zaja R, Loncar J, Fent K, Kovacevic R and Smital T (2015) Characterization of glutathione-S-transferases in zebrafish (Danio rerio). *Aquat Toxicol* **158**:50-62.

Grek C and Townsend DM (2014) Protein Disulfide Isomerase Superfamily in Disease and the Regulation of Apoptosis. *Endoplasmic Reticulum Stress Dis* **1**:4-17.

Guang MHZ, Kavanagh EL, Dunne LP, Dowling P, Zhang L, Lindsay S, Bazou D, Goh CY, Hanley C, Bianchi G, Anderson KC, O'Gorman P and McCann A (2019) Targeting Proteotoxic Stress in Cancer: A Review of the Role that Protein Quality Control Pathways Play in Oncogenesis. *Cancers (Basel)* **11**.

Henderson CJ, Smith AG, Ure J, Brown K, Bacon EJ and Wolf CR (1998) Increased skin tumorigenesis in mice lacking pi class glutathione S-transferases. *Proc Natl Acad Sci U S A* **95**:5275-5280.

Henderson CJ and Wolf CR (2011) Knockout and transgenic mice in glutathione transferase research. *Drug Metab Rev* **43**:152-164.

Howie AF, Forrester LM, Glancey MJ, Schlager JJ, Powis G, Beckett GJ, Hayes JD and Wolf CR (1990) Glutathione S-transferase and glutathione peroxidase expression in normal and tumour human tissues. *Carcinogenesis* **11**:451-458.

Kapp FG, Perlin JR, Hagedorn EJ, Gansner JM, Schwarz DE, O'Connell LA, Johnson NS, Amemiya C, Fisher DE, Wolfle U, Trompouki E, Niemeyer CM, Driever W and Zon LI (2018) Protection from UV light is an evolutionarily conserved feature of the haematopoietic niche. *Nature* **558**:445-448.

Li S, Pozhitkov A, Ryan RA, Manning CS, Brown-Peterson N and Brouwer M (2010) Constructing a fish metabolic network model. *Genome Biol* **11**:R115.

Liu L, Chen J, Cao M, Wang J and Wang S (2019) NO donor inhibits proliferation and induces apoptosis by targeting PI3K/AKT/mTOR and MEK/ERK pathways in hepatocellular carcinoma cells. *Cancer Chemother Pharmacol* **84**:1303-1314.

Maher P (2005) The effects of stress and aging on glutathione metabolism. *Ageing Res Rev* **4**:288-314.

Mavi PS, Singh S and Kumar A (2020) Reductive Stress: New Insights in Physiology and Drug Tolerance of Mycobacterium. *Antioxid Redox Signal* **32**:1348-1366.

Mohd Sakeh N, Md Razip NN, Mohd Ma'in FI, Abdul Bahari MN, Latif N, Akhtar MN, Balia Yusof ZN and Ahmad S (2020) Melanogenic Inhibition and Toxicity Assessment of Flavokawain A and B on B16/F10 Melanoma Cells and Zebrafish (Danio rerio). *Molecules* **25**.

Mukaigasa K, Tsujita T, Nguyen VT, Li L, Yagi H, Fuse Y, Nakajima-Takagi Y, Kato K, Yamamoto M and Kobayashi M (2018) Nrf2 activation attenuates genetic endoplasmic reticulum stress induced by a mutation in the phosphomannomutase 2 gene in zebrafish. *Proc Natl Acad Sci U S A* **115**:2758-2763.

Oda T, Kosuge Y, Arakawa M, Ishige K and Ito Y (2008) Distinct mechanism of cell death is responsible for tunicamycin-induced ER stress in SK-N-SH and SH-SY5Y cells. *Neurosci Res* **60**:29-39.

Okamura T, Antoun G, Keir ST, Friedman H, Bigner DD and Ali-Osman F (2015) Phosphorylation of Glutathione S-Transferase P1 (GSTP1) by Epidermal Growth Factor Receptor (EGFR) Promotes Formation of the GSTP1-c-Jun N-terminal kinase (JNK) Complex and Suppresses JNK Downstream Signaling and Apoptosis in Brain Tumor Cells. *J Biol Chem* **290**:30866-30878.

Park KH and Kim SH (2019) Low dose of chronic ethanol exposure in adult zebrafish induces hepatic steatosis and injury. *Biomed Pharmacother* **117**:109179.

Park KH, Ye ZW, Zhang J, Hammad SM, Townsend DM, Rockey DC and Kim SH (2019a) 3-ketodihydrosphingosine reductase mutation induces steatosis and hepatic injury in zebrafish. *Sci Rep* **9**:1138.

Park KH, Ye ZW, Zhang J and Kim SH (2019b) Palmitic Acid-Enriched Diet Induces Hepatic Steatosis and Injury in Adult Zebrafish. *Zebrafish* **16**:497-504.

Perez-Torres I, Guarner-Lans V and Rubio-Ruiz ME (2017) Reductive Stress in Inflammation-Associated Diseases and the Pro-Oxidant Effect of Antioxidant Agents. *Int J Mol Sci* **18**.

Peris E, Micallef P, Paul A, Palsdottir V, Enejder A, Bauza-Thorbrugge M, Olofsson CS and Wernstedt Asterholm I (2019) Antioxidant treatment induces reductive stress associated with mitochondrial dysfunction in adipocytes. *J Biol Chem* **294**:2340-2352.

Raijmakers MT, Steegers EA and Peters WH (2001) Glutathione S-transferases and thiol concentrations in embryonic and early fetal tissues. *Hum Reprod* **16**:2445-2450.

Rajasekaran NS, Connell P, Christians ES, Yan LJ, Taylor RP, Orosz A, Zhang XQ, Stevenson TJ, Peshock RM, Leopold JA, Barry WH, Loscalzo J, Odelberg SJ and Benjamin IJ (2007) Human alpha B-crystallin mutation causes oxido-reductive stress and protein aggregation cardiomyopathy in mice. *Cell* **130**:427-439.

Saito S, Furuno A, Sakurai J, Sakamoto A, Park HR, Shin-Ya K, Tsuruo T and Tomida A (2009) Chemical genomics identifies the unfolded protein response as a target for selective cancer cell killing during glucose deprivation. *Cancer Res* **69**:4225-4234.

Sehgal P, Szalai P, Olesen C, Praetorius HA, Nissen P, Christensen SB, Engedal N and Moller JV (2017) Inhibition of the sarco/endoplasmic reticulum (ER) Ca(2+)-ATPase by thapsigargin analogs induces cell death via ER Ca(2+) depletion and the unfolded protein response. *J Biol Chem* **292**:19656-19673.

Suzuki T, Takagi Y, Osanai H, Li L, Takeuchi M, Katoh Y, Kobayashi M and Yamamoto M (2005) Pi class glutathione S-transferase genes are regulated by Nrf 2 through an evolutionarily conserved regulatory element in zebrafish. *Biochem J* **388**:65-73.

Tierbach A, Groh KJ, Schonenberger R, Schirmer K and Suter MJ (2018) Glutathione S-Transferase Protein Expression in Different Life Stages of Zebrafish (Danio rerio). *Toxicol Sci* **162**:702-712.

Townsend DM, Manevich Y, He L, Hutchens S, Pazoles CJ and Tew KD (2009a) Novel role for glutathione S-transferase pi. Regulator of protein S-Glutathionylation following oxidative and nitrosative stress. *J Biol Chem* **284**:436-445.

Townsend DM, Manevich Y, He L, Xiong Y, Bowers RR, Jr., Hutchens S and Tew KD (2009b) Nitrosative stress-induced s-glutathionylation of protein disulfide isomerase leads to activation of the unfolded protein response. *Cancer Res* **69**:7626-7634.

Wu X, Zhang L, Miao Y, Yang J, Wang X, Wang CC, Feng J and Wang L (2019) Homocysteine causes vascular endothelial dysfunction by disrupting endoplasmic reticulum redox homeostasis. *Redox Biol* **20**:46-59.

Xia W, Wang Y, Zhang Y, Ge X, Lv P, Cheng J and Wei J (2020) Endoplasmic reticulum stress induces growth retardation by inhibiting growth hormone IGF-I axis. *Growth Horm IGF Res* **55**:101341.

Xiong Y, Manevich Y, Tew KD and Townsend DM (2012) S-Glutathionylation of Protein Disulfide Isomerase Regulates Estrogen Receptor alpha Stability and Function. *Int J Cell Biol* **2012**:273549.

Ye ZW, Zhang J, Ancrum T, Manevich Y, Townsend DM and Tew KD (2017) Glutathione S-Transferase P-Mediated Protein S-Glutathionylation of Resident Endoplasmic Reticulum Proteins Influences Sensitivity to Drug-Induced Unfolded Protein Response. *Antioxid Redox Signal* **26**:247-261.

Zhang J, Ye ZW, Chen W, Culpepper J, Jiang H, Ball LE, Mehrotra S, Blumental-Perry A, Tew KD and Townsend DM (2020) Altered redox regulation and S-glutathionylation of BiP contribute to bortezomib resistance in multiple myeloma. *Free Radic Biol Med* **160**:755-767.

Zhang J, Ye ZW, Gao P, Reyes L, Jones EE, Branham-O'Connor M, Blumer JB, Drake RR, Manevich Y, Townsend DM and Tew KD (2014) Glutathione S-transferase P influences redox and migration pathways in bone marrow. *PLoS One* **9**:e107478.

Zhang J, Ye ZW, Singh S, Townsend DM and Tew KD (2018) An evolving understanding of the S-glutathionylation cycle in pathways of redox regulation. *Free Radic Biol Med* **120**:204-216.

Zhang L, Zhang J, Ye Z, Manevich Y, Ball LE, Bethard JR, Jiang YL, Broome AM, Dalton AC, Wang GY, Townsend DM and Tew KD (2019) Isoflavone ME-344 Disrupts Redox Homeostasis and Mitochondrial Function by Targeting Heme Oxygenase 1. *Cancer Res* **79**:4072-4085.

Zon LI and Peterson RT (2005) In vivo drug discovery in the zebrafish. *Nat Rev Drug Discov* **4**:35-44.

JPET Fast Forward. Published on January 29, 2021 as DOI: 10.1124/jpet.120.000417
This article has not been copyedited and formatted. The final version may differ from this version.

Footnotes

Funding

This work was supported by grants from the National Institutes of Health (5P20GM103542-09 - COBRE in Oxidants, Redox Balance and Stress Signaling) and support from the South Carolina Centers of Excellence program and was conducted in a facility constructed with the support from the National Institutes of Health, Grant Number C06 RR015455 from the Extramural Research Facilities Program of the National Center for Research Resources.

JPET Fast Forward. Published on January 29, 2021 as DOI: 10.1124/jpet.120.000417
This article has not been copyedited and formatted. The final version may differ from this version.

Figure Legends

Figure 1. Generation of *gstp1* KO zebrafish. (**A**) *Gstp1*cri mutant has 11 bp deletion. Deleted nucleotides are shown in red in WT. Relative levels of mRNA expression (**B**) and protein expression (**C**) of Gstp1/2 in WT and *gstp1* KO zebrafish. (**D**) GST activity in WT and *gstp1* KO zebrafish. **p < 0.01, ***p < 0.001 vs. WT by 2 tailed t tests.

Figure 2. Drug toxicities in WT and *gstp1* KO zebrafish larvae. Dose-dependent survival curves for WT and *gstp1* KO zebrafish larvae. Larvae at 4 dpf were exposed to (**A**) TuM, (**B**) ThG and (**C**) PABA/NO for 24 h. Each point is the average of triplicate measurements and each measurement contains data from 10 larvae ± standard deviations (SD) (μM).

Figure 3. Zebrafish larvae malformation assays. A. D. Representative views of larval malformations caused by TuM, ThG and PABA/NO after 16 h and 24 h. Total malformations (**B. E.**) and body length (**C. F.**) for 16 h and 24 h are presented as mean ± SD for three replicates per treatment (n=10 random larvae per replicate) in scatter plots.

Figure 4. Drug effects on redox homeostasis.

TuM: (**A**) GSH levels, (**B**) GSSG levels, (**C**) GSH/GSSG ratios, (**D**) Protein thiol, (**E**) Intracellular ROS, and (**F**) mRNA expression of *gclc, gclm* and *gr*. Data are derived from three independent experiments presented as means ± SD in scatter plots. *p < 0.05 vs. WT untreated control, #p < 0.05, ##p < 0.01 vs. KO untreated control by one-way ANOVA followed by Newman-Keuls as a post-test.

ThG: (**G**) GSH levels, (**H**) GSSG levels, (**I**) GSH/GSSG ratios, (**J**) Protein thiol, (**K**) Intracellular ROS, and (**L**) mRNA expression of *gclc, gclm* and *gr*. Data are derived from three independent experiments presented as means ± SD in scatter plots. *p < 0.05, **p < 0.01 vs. WT untreated

JPET Fast Forward. Published on January 29, 2021 as DOI: 10.1124/jpet.120.000417
This article has not been copyedited and formatted. The final version may differ from this version.

control, #p < 0.05, ##p < 0.01 vs. KO untreated control by one-way ANOVA followed by Newman-Keuls as a post-test.

PABA/NO: (**M**) GSH levels, (**N**) GSSG levels, (**O**) GSH/GSSG ratios, (**P**) Protein thiol, (**Q**) Intracellular ROS, and (**R**) mRNA expression of *gclc, gclm* and *gr*. Data are derived from three independent experiments presented as means ± SD in scatter plots. *p < 0.05 vs. WT untreated control, #p < 0.05, ##p < 0.01 vs. KO untreated control by one-way ANOVA followed by Newman-Keuls as a post-test.

Figure 5. Heat map showing drug-induced changes in expression of oxidative stress and ER stress response genes. Larvae at 4 dpf were exposed to TuM (4 μM), ThG (0.75 μM) and PABA/NO (4 μM) for 24 h. Shown are fold-changes in gene expression after drug treatment relative to WT untreated larvae with mean values set at 1. Relative gene expression quantification was based on the CT method ($2^{\Delta\Delta Ct}$), with normalization of the raw data to the housekeeping gene (*gapdh*). Data are derived from three independent experiments presented as means ± SD in heatmap. *p < 0.05, **p < 0.01, ***p < 0.001 vs. the WT untreated control, #p < 0.05, ##p < 0.01, ###p < 0.001 vs. the KO untreated control by one-way ANOVA followed by Newman-Keuls as a post-test.

Figure 6. Oxidative stress protein expression. Larvae at 4 dpf were exposed to TuM (4 μM), ThG (0.75 μM) and PABA/NO (4 μM) for 24 h. **A.** Proteins were separated by SDS-PAGE and evaluated by immunoblots. **B.** Protein expression before and after treatment was quantified by ImageJ software. Fold-changes in protein expression after drug treatment relative to WT untreated larvae with mean values set at 1. Relative protein expression quantification was normalized to GAPDH. Data are derived from three independent experiments, presented as means ± SD in the scatter plots. *p < 0.05, **p < 0.01 vs. the WT untreated control, #p < 0.05 vs. KO untreated control by one-way ANOVA followed by Newman-Keuls as a post-test.

JPET Fast Forward. Published on January 29, 2021 as DOI: 10.1124/jpet.120.000417
This article has not been copyedited and formatted. The final version may differ from this version.

Figure 7. ER stress/UPR protein expression. Larvae at 4 dpf were exposed to TuM (4 μM), ThG (0.75 μM) and PABA/NO (4 μM) for 24 h. **A-C.** Protein expression before and after treatment was quantified by ImageJ software. Fold-changes in protein expression after drug treatment relative to WT untreated larvae with mean values set at 1. Relative protein expression quantification was normalized to GAPDH. Data are derived from three independent experiments presented as means ± SD in scatter plots. *p < 0.05, **p < 0.01, ***p < 0.001 vs. the WT untreated control, #p < 0.05, ##p < 0.01, ###p < 0.001 vs. KO untreated control by one-way ANOVA followed by Newman-Keuls as a post-test.

JPET Fast Forward. Published on January 29, 2021 as DOI: 10.1124/jpet.120.000417
This article has not been copyedited and formatted. The final version may differ from this version.

Table 1. LC_{50} values in zebrafish and mice.

Drugs	*Gstp1* zebrafish, μmol/L		BMDDCs mouse, μmol/L (Ye et al., 2017)		Mice, mg/kg	*PMM2* mutation zebrafish, μmol/L
	WT	KO	WT	KO		
TuM	7.97±0.77	5.96±0.69	0.256±0.006	0.113±0.011	2 (Xia et al., 2020)	6 (Mukaigasa et al., 2018)
ThG	1.47±0.12	0.98±0.09	0.122±0.028	0.017±0.001	0.2 (Cheng et al., 2019)	2 (Mukaigasa et al., 2018)
PABA/NO	8.12±0.82	6.05±0.58	NA	NA	2 (Liu et al., 2019)	NA

BMDDCs, bone marrow-derived dendritic cells; LC_{50}, 50% lethal concentrations.

JPET Fast Forward. Published on January 29, 2021 as DOI: 10.1124/jpet.120.000417
This article has not been copyedited and formatted. The final version may differ from this version.

Table 2. Drug-induced changes in gene expression of oxidative stress and ER stress/UPR in WT and *gstp1* KO zebrafish larvae.

	WT				KO			
	Ctrl	TuM	ThG	PABA/NO	Ctrl	TuM	ThG	PABA/NO
nrf2a	1.00±0.04	1.46±0.11*	1.03±0.04	1.25±0.09*	1.01±0.09	1.67±0.08#	1.43±0.05#	1.52±0.01#
sod2	1.00±0.09	1.17±0.10	0.99±0.10	1.27±0.11*	0.90±0.15	1.70±0.19#	1.27±0.03#	1.92±0.17#
gstp1/2	1.00±0.06	1.72±0.07*	1.69±0.30	1.68±0.13*	0.31±0.01*	0.75±0.03#	0.49±0.06#	0.75±0.03#
bip	1.00±0.06	2.87±0.28*	1.11±0.05	1.27±0.04*	0.51±0.04*	1.50±0.14#	0.51±0.04#	1.39±0.01#
dnajc3	1.00±0.17	1.66±0.17*	1.79±0.07	1.00±0.03	0.83±0.11	2.88±0.38#	1.60±0.18#	1.92±0.23#
grp94	1.00±0.08	2.31±0.11*	1.33±0.12*	1.32±0.14*	0.95±0.06	2.41±0.19#	1.27±0.09#	1.77±0.07#
ire1	1.00±0.02	1.17±0.01	1.56±0.15*	1.18±0.06	0.73±0.02*	1.18±0.06#	0.79±0.10	1.43±0.11#
perk	1.00±0.20	1.45±0.18	0.91±0.10	0.77±0.01	0.82±0.03	0.71±0.08	1.38±0.04#	0.79±0.01
atf6	1.00±0.20	1.00±0.19	0.91±0.20	0.82±0.02	0.35±0.23*	0.47±0.01	0.48±0.19	0.33±0.01
xbp1-u	1.00±0.06	1.04±0.06	1.11±0.02	1.17±0.05	0.80±0.04*	0.97±0.05#	0.61±0.02#	0.90±0.10
xbp1-s	1.00±0.07	1.17±0.27	1.13±0.03	1.16±0.06	0.61±0.04*	1.78±0.03#	0.48±0.02#	1.27±0.05#
atf4	1.00±0.05	1.07±0.04	1.15±0.03	0.88±0.06	0.79±0.07*	1.61±0.13#	1.38±0.07#	1.27±0.03#
chop	1.00±0.03	1.08±0.04	1.16±0.06	0.99±0.07	0.70±0.03*	1.26±0.04#	1.35±0.09#	1.32±0.09#
gadd45a	1.00±0.04	0.83±0.05	0.47±0.10*	0.91±0.02	0.74±0.01*	1.18±0.07#	1.08±0.12#	1.52±0.09#
edem1	1.00±0.07	1.25±0.13	1.67±0.09*	1.43±0.20	1.06±0.07	1.90±0.18#	1.44±0.20	1.61±0.21#
baxb	1.00±0.18	0.96±0.02	2.44±0.24*	1.32±0.20	1.10±0.04	1.67±0.11#	1.62±0.10#	2.20±0.10#
bida	1.00±0.03	1.09±0.12	2.01±0.26*	0.97±0.00	0.97±0.17	1.78±0.29#	1.43±0.28	2.15±0.21#
bim	1.00±0.14	0.96±0.11	2.53±0.08*	1.35±0.12*	1.14±0.03	1.83±0.22#	1.30±0.13	2.11±0.22#

*$p < 0.05$ vs. the WT untreated control, #$p < 0.05$ vs. the KO untreated control by one-way ANOVA followed by Newman-Keuls as a post-test. See Fig. 5 for detailed-statistical significance.

JPET Fast Forward. Published on January 29, 2021 as DOI: 10.1124/jpet.120.000417
This article has not been copyedited and formatted. The final version may differ from this version.

Figure 1

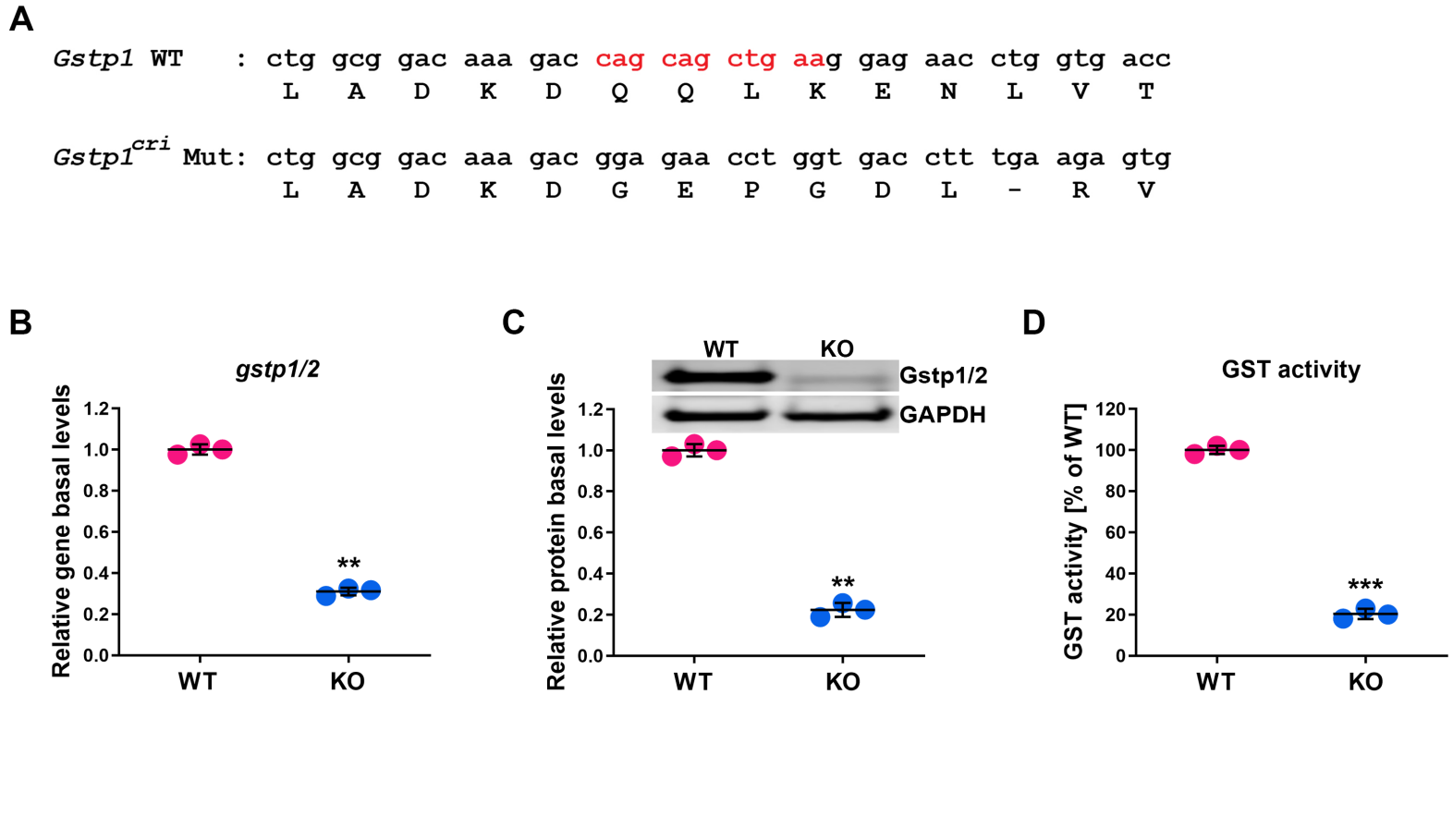

Figure 2

JPET Fast Forward. Published on January 29, 2021 as DOI: 10.1124/jpet.120.000417
This article has not been copyedited and formatted. The final version may differ from this version.

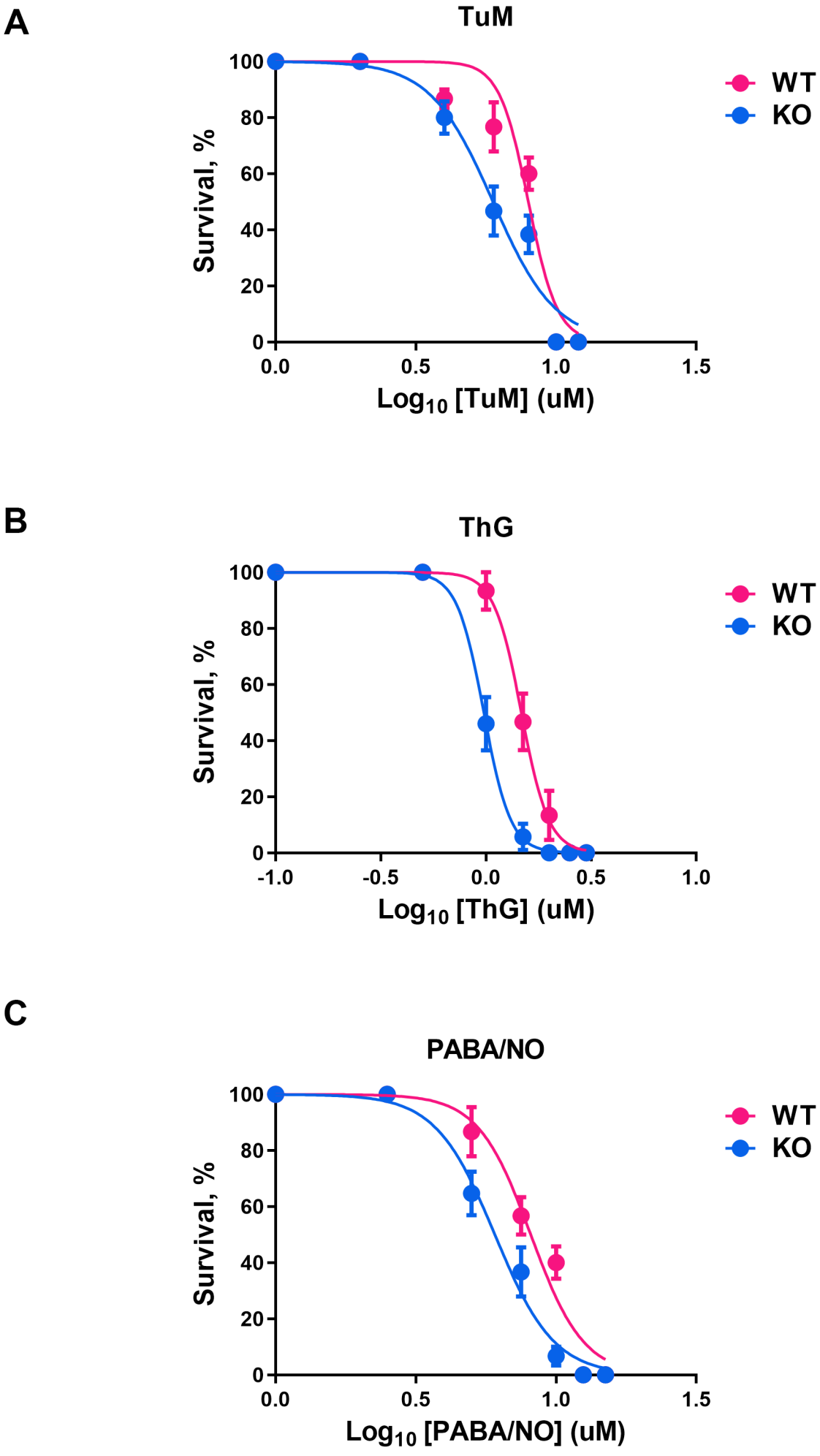

JPET Fast Forward. Published on January 29, 2021 as DOI: 10.1124/jpet.120.000417
This article has not been copyedited and formatted. The final version may differ from this version.

Figure 3 A-C

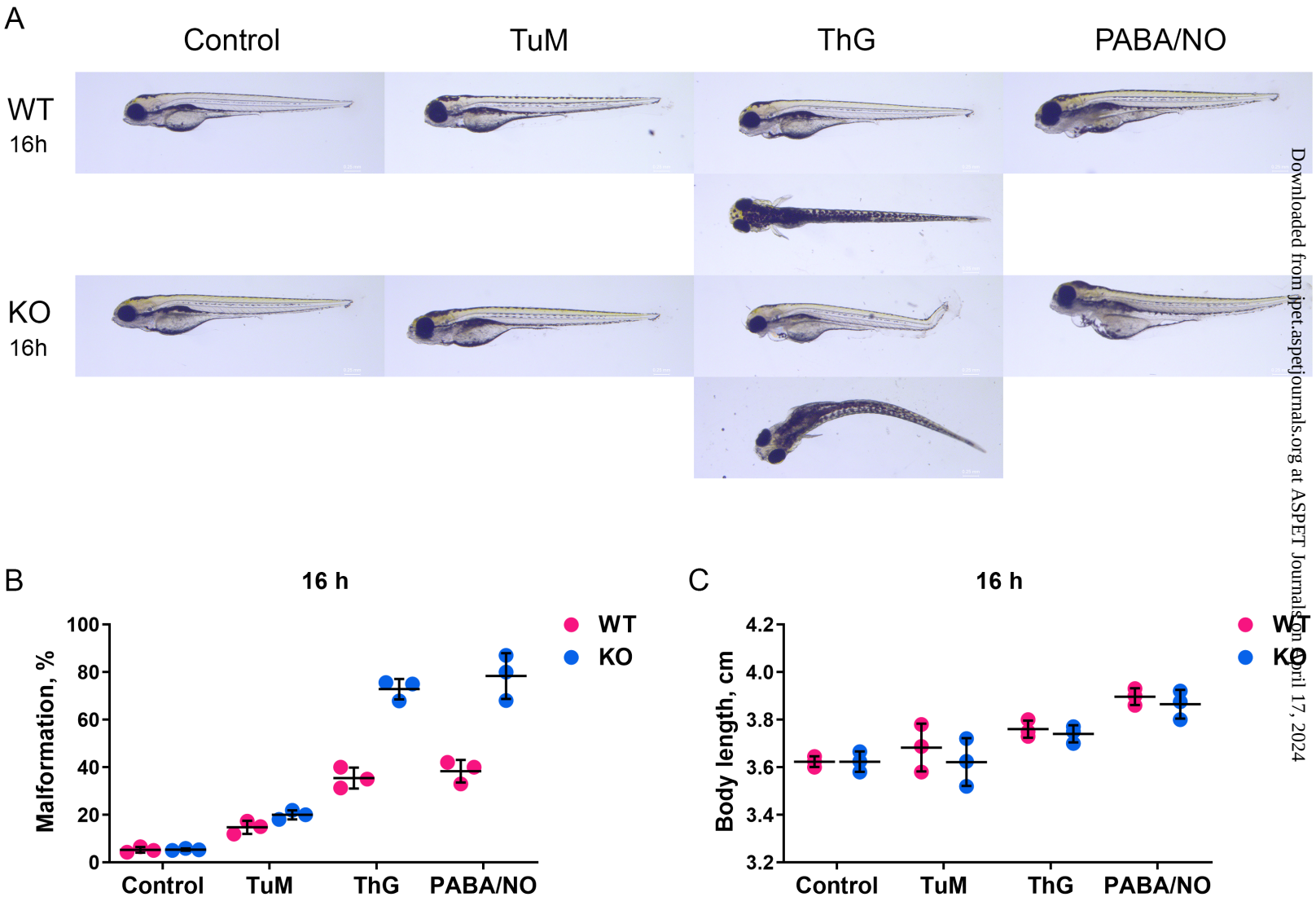

JPET Fast Forward. Published on January 29, 2021 as DOI: 10.1124/jpet.120.000417
This article has not been copyedited and formatted. The final version may differ from this version.

Figure 3 D-F

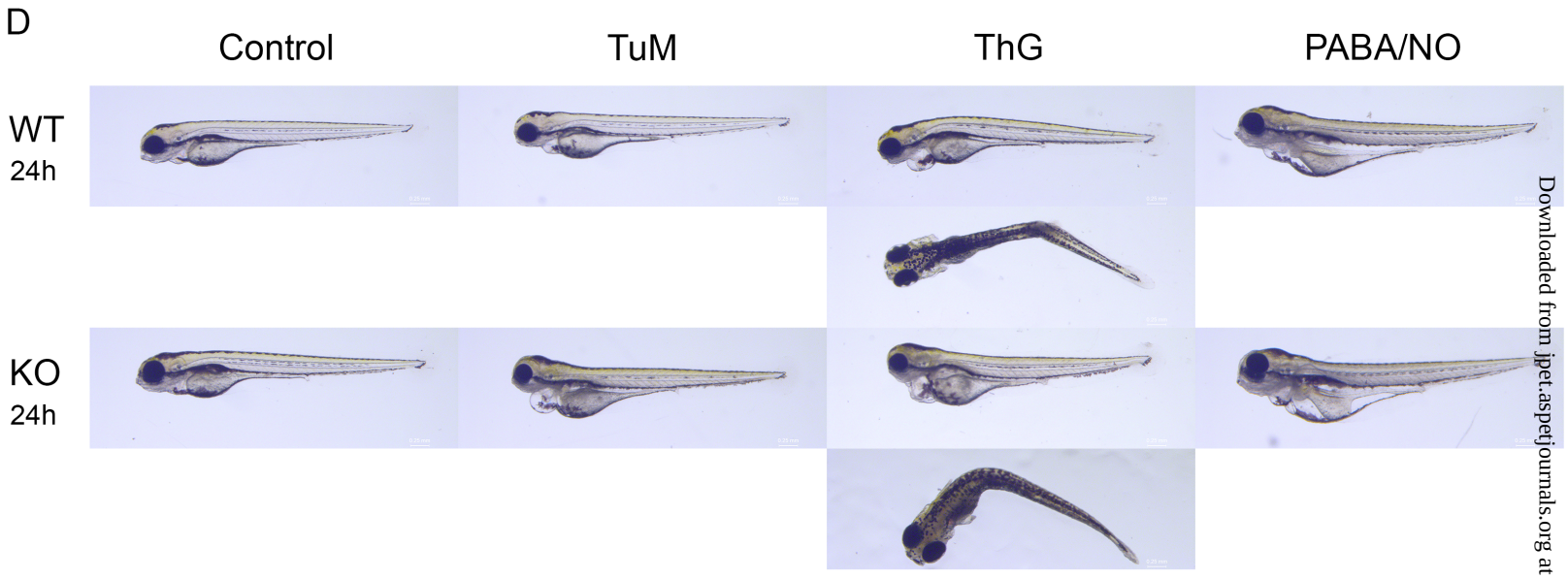

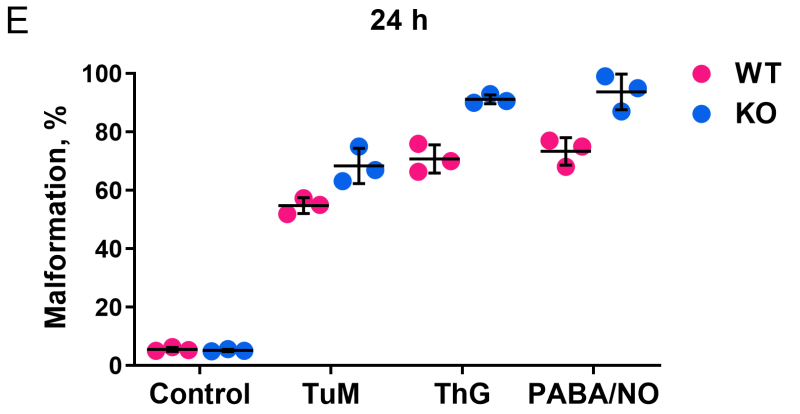

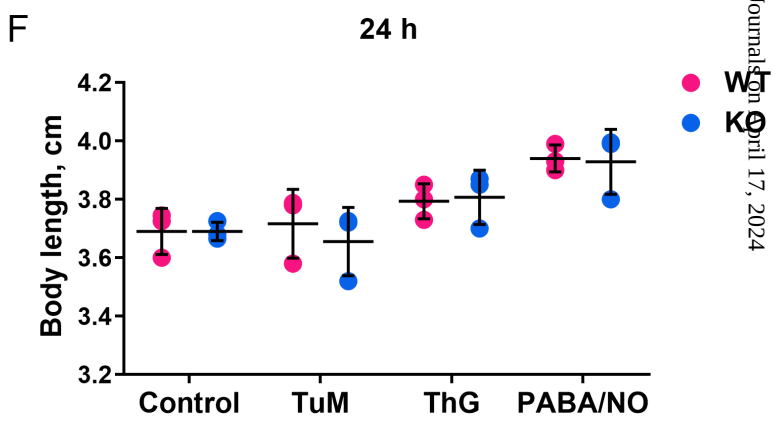

JPET Fast Forward. Published on January 29, 2021 as DOI: 10.1124/jpet.120.000417
This article has not been copyedited and formatted. The final version may differ from this version.

Figure 4A-F

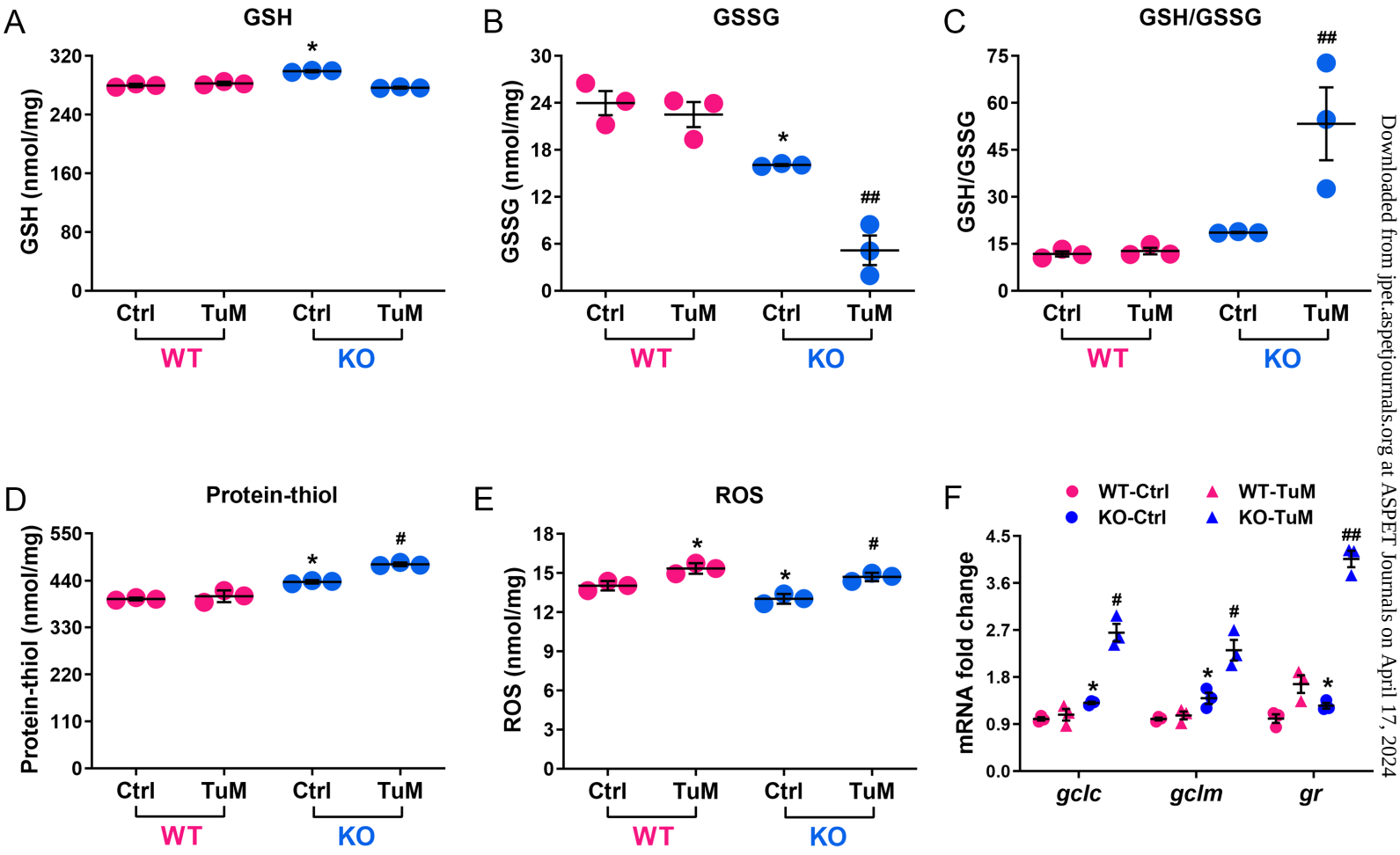

JPET Fast Forward. Published on January 29, 2021 as DOI: 10.1124/jpet.120.000417
This article has not been copyedited and formatted. The final version may differ from this version.

Figure 4G-L

ThG treatment

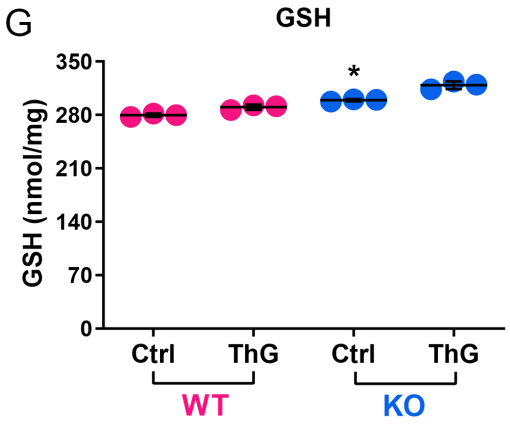

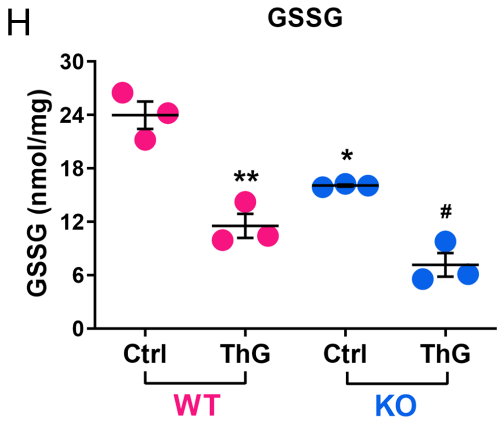

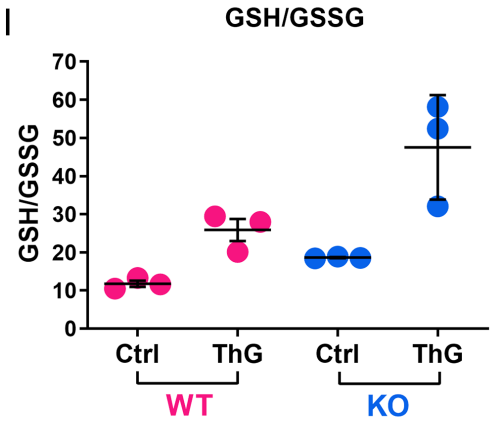

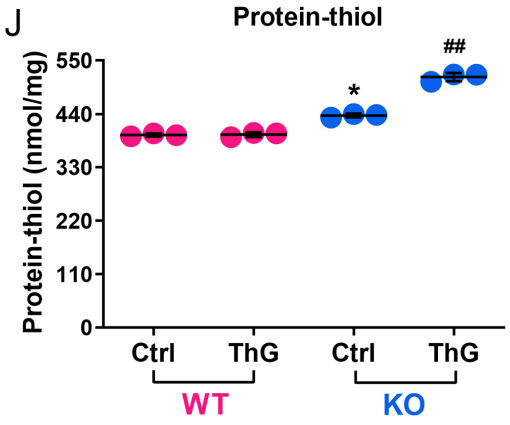

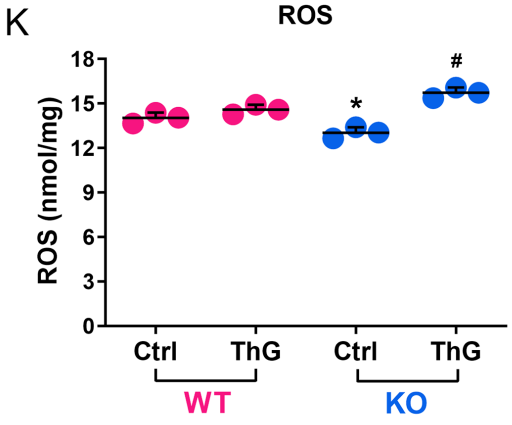

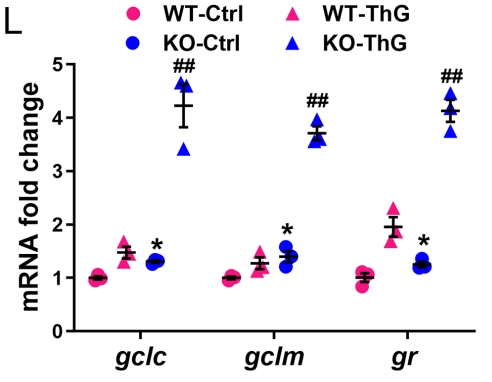

JPET Fast Forward. Published on January 29, 2021 as DOI: 10.1124/jpet.120.000417
This article has not been copyedited and formatted. The final version may differ from this version.

Figure 4M-R

PABA/NO treatment

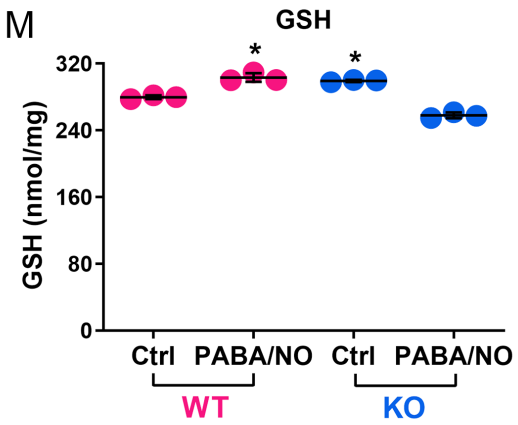

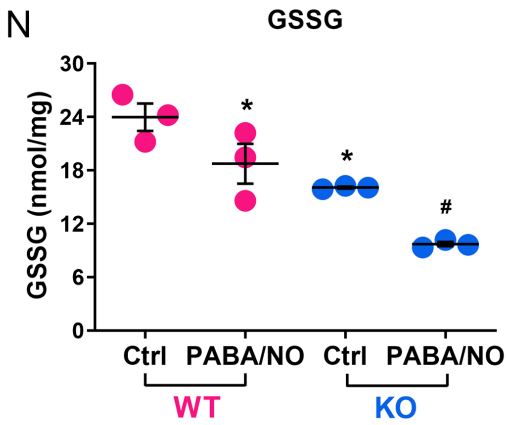

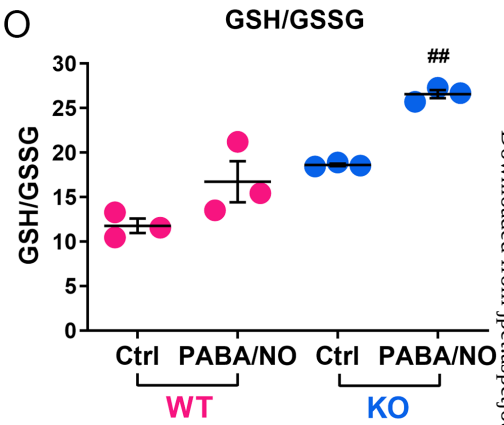

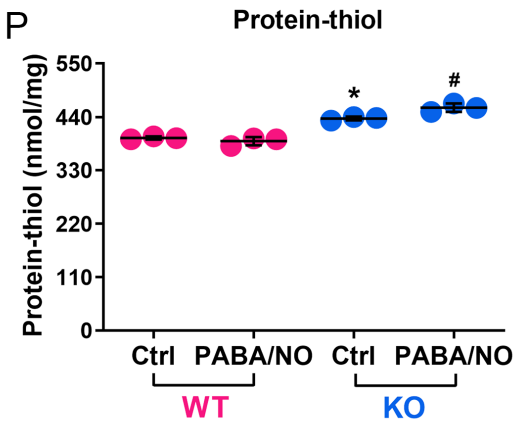

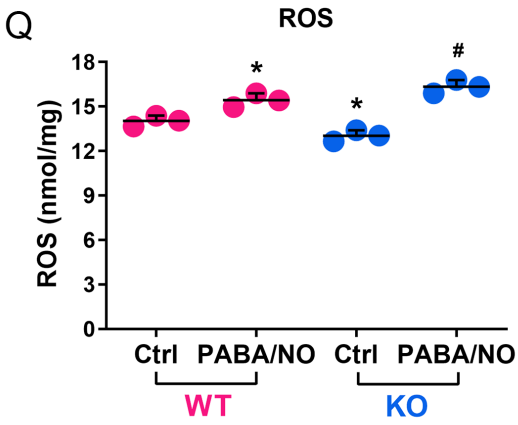

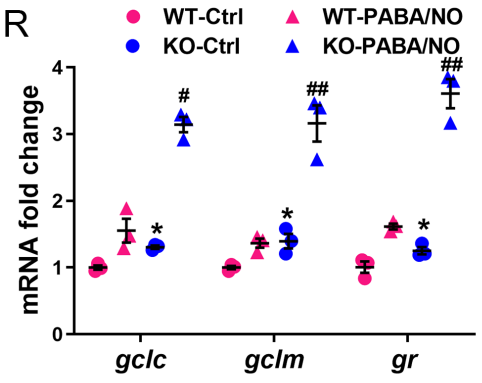

JPET Fast Forward. Published on January 29, 2021 as DOI: 10.1124/jpet.120.000417
This article has not been copyedited and formatted. The final version may differ from this version.

Figure 5

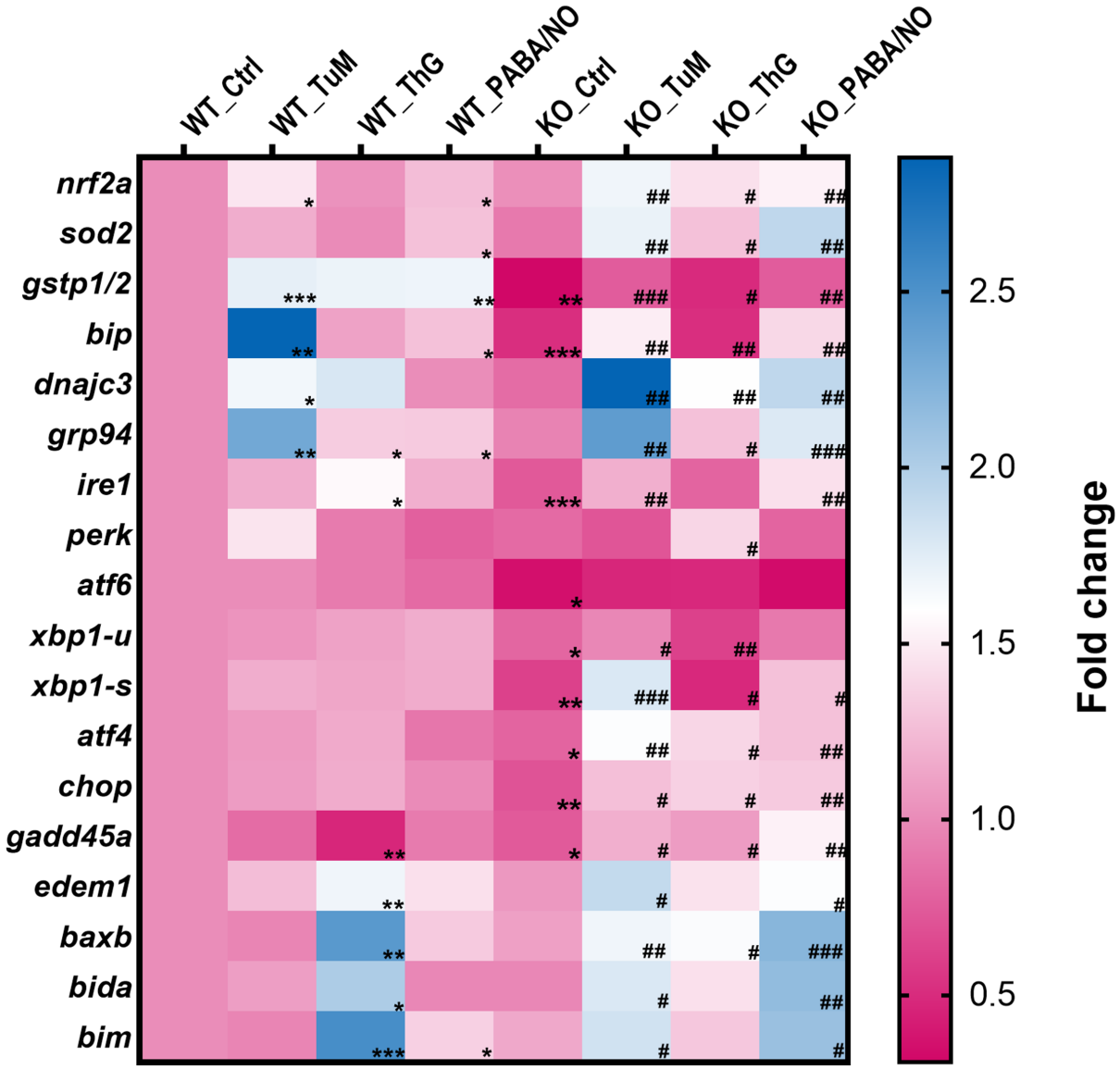

JPET Fast Forward. Published on January 29, 2021 as DOI: 10.1124/jpet.120.000417
This article has not been copyedited and formatted. The final version may differ from this version.

Figure 6

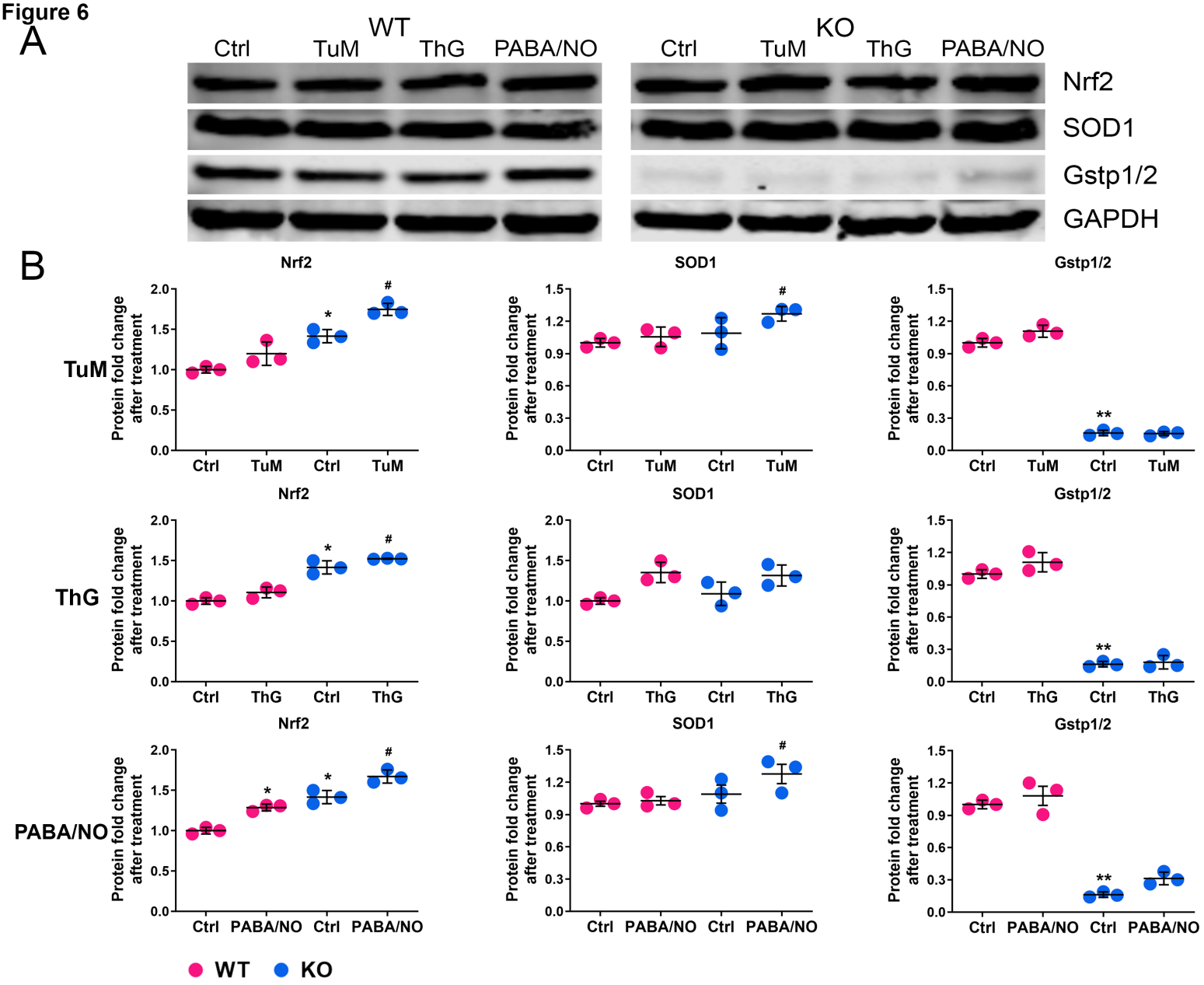

Figure 7

JPET Fast Forward. Published on January 29, 2021 as DOI: 10.1124/jpet.120.000417
This article has not been copyedited and formatted. The final version may differ from this version.